CHAPTER IV
RESULTS AND DISCUSSION

4.1 Adsorbent Characterization

The different activated carbons (AC, ACB, and ACP) were modified by three diferrent surface treatment methods including HNO_3 oxidation, amination without HNO_3 pre-oxidation, and amination with HNO_3 pre-oxidation.

The samples treated by oxidation alone were denoted as XXXOcc-tt, where "XXX" represents type of activated carbons, "O" represents Oxidation, "cc" represents concentration in molar and "tt" represents oxidation time in hour. The samples obtained by amination alone were denoted as XXXNyyy, where "N" represents Amination and "yyy" represents amination temperature. And the samples obtained by pre-oxidation followed by amination were denoted as XXXOcc-tt/Nyyy.

The untreated and treated activated carbons were characterized through texture and chemical characteristics. The textural properties were investigated by surface area analyzer. Ultimate and XPS analyses were performed to study surface chemistry of the samples.

4.1.1 Textural Characterization

N_2 adsorption/desorption isotherms were undertaken at -196 °C on a Surface Area Analyzer (Sorptomatic) to determine textural characteristics of the samples. The Brunauer-Emmett-Teller (BET) method was applied to evaluated apparent surface area. The total pore volume was assessed from the N_2 adsorption at p/p^0 of 0.99, and the average micropore diameter was obtained by Horvath Kawazoe (HK) method.

The N_2 adsorption/desorption curves at -196 °C for AC samples before and after surface treatment were illustrated in Figure 4.1. The isotherm shape of untreated AC and all treated AC is type IV.

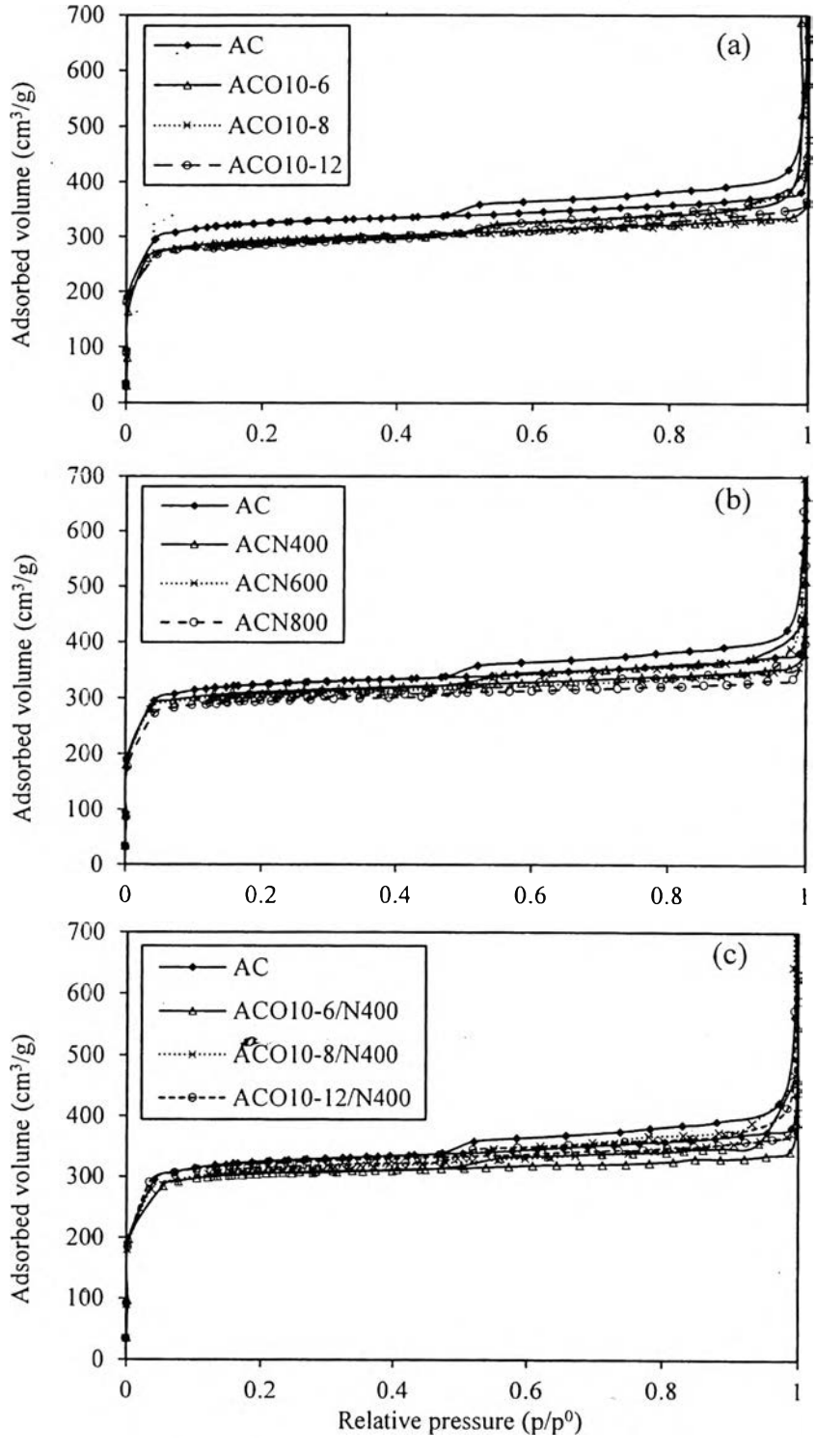

Figure 4.1 N_2 adsorption/desorption isotherms at -196 °C for AC treated by (a) HNO_3 oxidation, (b) amination without HNO_3 pre-oxidation, and (c) amination with HNO_3 pre-oxidation.

The type IV isotherm corresponds to combination between micro- and meso-porosity (Sing *et al.*, 1985) as observed from a hysteresis loop at p/p^0 above 0.4. This loop is caused by the mesopores with a capillary condensation (Su *et al.*, 2009).

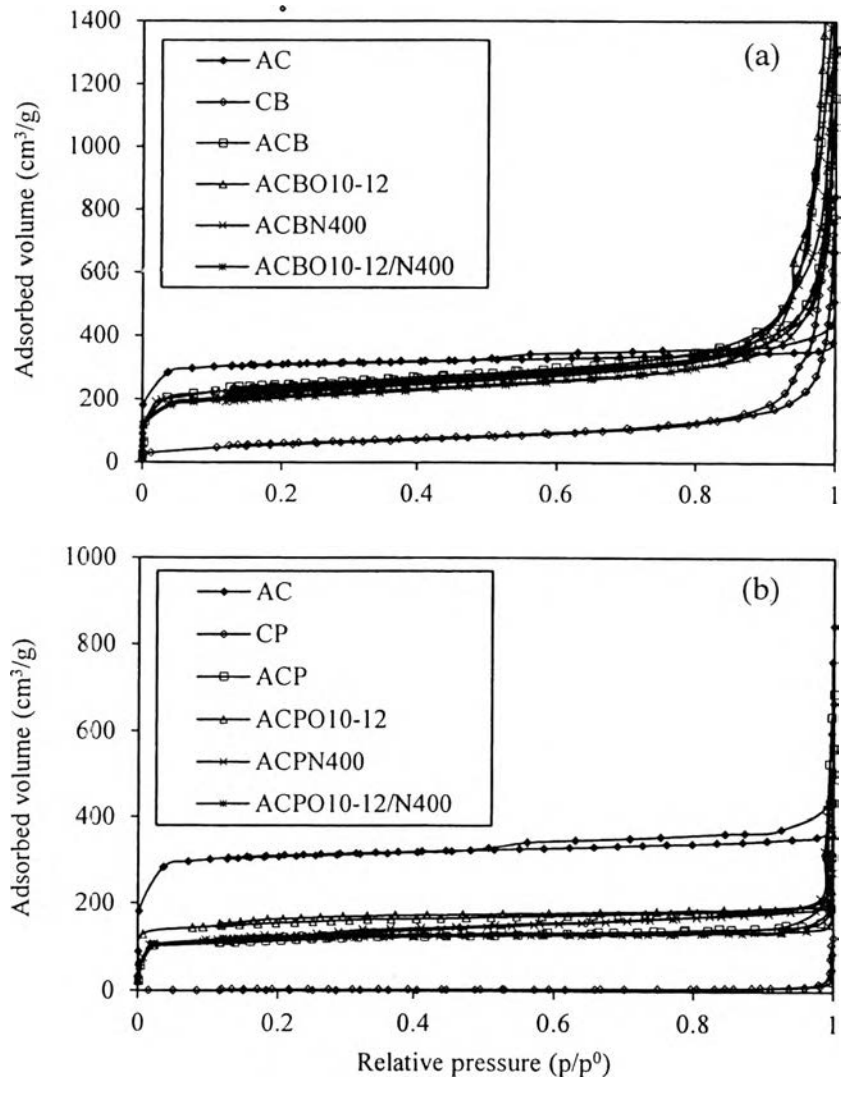

Figure 4.2 N_2 adsorption/desorption isotherms at -196 °C for (a) CB and (b) CP carbons before and after modification.

Figure 4.2 exhibits the N_2 adsorption/desorption isotherms at -196 °C of the CNS before and after modification compared to AC. The greatest N_2 adsorption was obtained for the AC, which exhibited highest apparent surface area and mi-

cropore volume. It was observed that the N_2 adsorption isotherm of all activated CNS samples exhibited similar shape to that of the AC (Type IV). The shift in the isotherm of all activated CNS samples indicates that the porous development of both parent carbons was promoted after the carbonization and activation process.

Table 4.1 summarizes the apparent surface area (S_{BET}), micropore volume (V_{micro}), mesopore volume (V_{meso}), total pore volume (V_{total}), and average micropore diameter (D) of the studied samples.

Table 4.1 Textural parameters of the studied samples

Sample	S_{BET} (m^2/g)	V_{micro} (cm^3/g)	V_{meso} (cm^3/g)	V_{total} (cm^3/g)	D (nm)
AC	982	0.512	0.146	0.672	0.79
ACO10-6	893	0.465	0.130	0.560	0.77
ACO10-8	892	0.462	0.147	0.560	0.70
ACO10-12	883	0.460	0.157	0.564	0.75
ACN400	947	0.491	0.138	0.590	0.70
ACN600	928	0.482	0.130	0.551	0.71
ACN800	903	0.469	0.110	0.520	0.70
ACO10-6/N400	948	0.479	0.113	0.529	0.72
ACO10-8/N400	954	0.488	0.165	0.569	0.72
ACO10-12/N400	963	0.506	0.126	0.578	0.74
CB	202	0.101	0.436	1.118	1.07
ACB	770	0.395	0.596	1.577	0.84
ACBO10-12	715	0.365	0.710	2.424	0.69
ACBN400	750	0.396	0.589	1.456	0.73
ACBO10-12/N400	671	0.352	0.681	1.835	0.77
CP	8	0.003	0.011	0.079	1.85
ACP	355	0.191	0.489	0.673	0.89
ACPO10-12	490	0.252	0.038	0.361	0.74
ACPN400	389	0.208	0.096	0.311	0.84
ACPO10-12/N400	365	0.190	0.031	0.482	0.79

The S_{BET}, V_{total}, V_{micro}, V_{meso}, and D of AC were 982 m^2/g, 0.672 cm^3/g, 0.512 cm^3/g, 0.146 cm^3/g, and 0.79 nm, respectively. It is seen that the AC sample consisted mostly of micropores and revealed the presence of some mesopores (possessed micropore volume approximately 76 % of total pore volume), while the pore volume of CB and CP carbons was mainly mesopore. The porous structure of the CB and CP samples was developed after the carbonization and activation processes, resulting in the increase of apparent surface area, micropore and total pore volume. The S_{BET}, V_{micro}, and V_{total} of ACB carbon were 770 m^2/g, 0.395 cm^3/g, and 1.577 cm^3/g. Whereas S_{BET}, V_{micro}, and V_{total} of ACP carbon were 355 m^2/g, 0.191 cm^3/g, and 0.673 cm^3/g. It can be observed that the ACB sample owed superior porous properties as compared to the ACP sample. However, this improvement in porosity still resulted in the relatively lower surface area and micropore volume than that of the commercial activated carbon (AC). It is noted that ACB sample constitutes 25 % micropores and 38 % mesopores while the ACP sample contains 28 % micropores and 72 % mesopores. Therefore, the majority of pore types in CNS are in mesoporous ranges. For the sample treated by various treatment approaches, the porous properties of the samples were not significantly changed by the surface treatment.

4.1.2 Chemical Characterization

4.1.2.1 Ultimate Analysis

Table 4.2 shows the results of ultimate analysis of all samples. To examine the amount of carbon, hydrogen, nitrogen, and oxygen present in the carbon samples, ultimate analysis was performed on a CHN elemental analyzer. The amount of each element was represented as a weight percentage. The oxygen content was calculated by the difference.

As observed from Table 4.2, the AC, CB, and CP samples present carbon compositions of 87.72 wt.%, 87.96 wt.%, and 79.40 wt.%, respectively. After carbonization and activation processes of CB and CP, the carbon contents were increased to 92.6 wt.% and 85.08 wt.%, respectively. During the carbonization process, volatile matters evolved from the starting materials resulting in the decrease in hydrogen and nitrogen contents and, therefore, increase in the amount of carbon

content. However, the increase of oxygen content was obtained after carbonization and activation. This increase could be due to the occurrence of some chemisorption of oxygen species on the carbon surface during activation with CO_2 (Plaza *et al.*, 2009a). The ACP sample contains nitrogen up to 5.22 wt.%, whereas there is no nitrogen present in AC and ACB. This difference is responsible to their starting carbon. The ACP carbon was prepared from pyridine-derived carbon nano spheres (CP) with a nitrogen content of 16.51 wt.%.

Table 4.2 Ultimate analysis of the studied samples

Sample	Ultimate Analysis (wt.%)			
	C	H	N	O
AC	87.72	0.59	0.00	11.69
ACO10-6	81.52	0.64	0.97	16.92
ACO10-8	80.03	0.72	1.01	18.24
ACO10-12	79.03	0.80	1.06	19.11
ACN400	87.82	0.57	1.20	10.41
ACN600	87.53	0.56	1.09	10.82
ACN800	87.63	0.55	0.27	11.55
ACO10-6/N400	83.22	0.89	1.93	13.96
ACO10-8/N400	83.13	0.83	2.56	13.48
ACO10-12/N400	82.73	0.74	3.14	13.39
CB	87.96	12.04	0.00	0.00
ACB	92.60	3.54	0.00	3.86
ACBO10-12	84.35	4.13	1.05	10.47
ACBN400	94.25	2.18	1.23	2.34
ACBO10-12/N400	89.06	1.14	3.59	6.21
CP	79.40	4.09	16.51	0.00
ACP	85.08	0.74	5.22	8.96
ACPO10-12	78.00	1.15	5.45	15.40
ACPN400	85.47	0.64	6.19	7.70
ACPO10-12/N400	78.59	1.06	7.59	12.76

After the surface treatment of all activated carbons by oxidation, an increase of oxygen content was observed. The surface treatment of AC by HNO_3 oxidation for various durations resulted in the enhanced of oxygen contents from 11.69 wt.% of untreated AC to 16.92 wt.%, 18.24 wt.% and 19.11 wt.% of the AC oxidized for 6, 8 and 12 hours, respectively. It is noted that the longer the oxidation length, the higher the oxygen content was observed. The enhancement of oxygen amount of the oxidized samples attributed to the formation of oxygen surface groups created on the carbon surface via the HNO_3 oxidation. Furthermore, it can be noticed that the treatment by oxidation caused the increasing of nitrogen content of the activated carbons. This observation may be related to the formation of nitro and nitrate groups formed by HNO_3 oxidation (Plaza *et al.*, 2013). In the case of activated carbons treated by amination, a small increase in the amount of nitrogen was observed. For the amination of AC at various temperatures, the AC aminated at 400 °C gave the largest nitrogen incorporated (1.20 wt.%). The higher the aminated temperature, the lower the amount of nitrogen was introduced. It can be clearly seen that the pre-oxidation prior to amination has significantly improved the amount of nitrogen incorporated. The amount of nitrogen content was enhanced from 1.20 wt.% to 1.93 wt.%, 2.56 wt.%, and 3.14 wt.% of ACO10-6/N400, ACO10-8/N400, and ACO10-12/N400, respectively. The highest nitrogen content, i.e. 3.14 wt.% was observed for the sample treated by 400 °C amination with the highest severity of HNO_3 pre-oxidation (ACO10-12/N400). It could be concluded that the more severity of the oxidation, the higher the amount of nitrogen could be introduced. This observation has confirmed that the formation of oxygen functional groups introduced by oxidation on the carbon surface prior to ammonia treatment can enhance the amount of nitrogen functionalities incorporated during amination. During heat treatment under NH_3 gas, the NH_3 decomposes to the formation of the free radicals such as NH_2, NH, and H. These free radicals can attach to oxygen containing functionalities present on carbon surface to form various nitrogen surface groups (Febo *et al.*, 2002; Shafeeyan *et al.*, 2010). Due to the consumption of surface oxides to form nitrogen groups during amination, the decrease of oxygen content for aminated samples was observed (Pe-

vida *et al.*, 2008a). Nevertheless, an XPS analysis was conducted to further examine the nature of surface functional groups of the treated samples.

4.1.2.2 X-ray Photoelectron Spectroscopy

High resolution XPS spectra of C1s, O1s and N1s regions was deconvoluted and analyzed to investigate the change of surface chemistry during surface treatment. The list of binding energies and corresponding assignments obtained by deconvolution is given in Tables 4.3 to 4.5. The amount of various species present on the sample was compared as peak area percentage determined from peak fitting.

The C1s spectra could be deconvoluted to six components located at the binding energy of 284.3, 285.0, 285.4, 285.8, 286.6, and 289.2 eV. These different binding energies were attributed to graphite at 284.3 eV, aliphatics at 285.0 eV, carbons linked to nitrogen at 285.4, hydroxyl/ether at 285.8 eV, carbonyl at 286.6 eV, and esters/lactones/anhydrides/acids/hydroxyl at 289.2 eV (Burg *et al.*, 2002; Plaza *et al.*, 2013). The graphitic carbon (BE = 284.3) was the dominant carbon functional group found on all samples, as shown in the Tables 4.3 to 4.5. The CP sample revealed the presence of peak at 285.4 eV corresponded to their carbon atoms bonded to nitrogen due to the presence of nitrogen atoms in the aromatic structure of the original pyridine precursor. After carbonization and activation of CB and CP samples, the component of graphitic carbon was decrease with the generation of surface functional groups containing carbon-oxygen bonds (László *et al.*, 2001). Moreover, it can be observed that the graphitic carbon percentage was lower after surface treatment. This could be related to the increase of carbon-oxygen groups (BE = 285.4, 285.8, and 286.6) formed by oxidation and the presence of carbon-nitrogen bonds (BE = 285.4) incorporated by amination.

The fitting peak of O1s spectrum confirmed the existence of oxygen surface groups on the sample treated with HNO_3 at the binding energy of 530.3, 531.3, 532.1, 532.9, 533.6, and 534.9 eV, which correspond to oxides, carbonyl/carboxyl, ketones/lactones/acids/esters, hydroxyl/carboxyl, hydroxyl attached to aromatic ring/oxygen in bridge (esters), and adsorbed water, respectively (Burg *et al.*, 2002; Plaza *et al.*, 2013). The oxidation led to an increase in oxygen functional groups especially the peak at 531.3 eV (assigned to carbonyl or carboxyl groups).

This indicated that carbonyl or carboxyl groups have successfully created by HNO_3 oxidation. It was reported that these acid functionalities present affinity toward CO_2 especially for carboxyl group (Plaza *et al.*, 2013).

The deconvolution of N1s peaks showed that the nitrogen functionalities incorporated by amination with and without pre-oxidation were in the formed of pyridinic (BE = 398.1 eV), pyridinic/imine (BE = 398.9 eV), imine/amide/amine (BE = 399.8 eV), pyrrolic/pyridonic (BE = 400.7 eV), quaternary nitrogen (BE = 401.4 eV), and pyridine-N-oxide (BE = 402.8 eV) (Arenillas *et al.*, 2005b; Pietrzak *et al.*, 2009; Plaza *et al.*, 2013) The main nitrogen functional groups introduced were pyrrolic and pyridonic groups (BE = 400.7 eV), which corresponded to the strong basic nature on the carbon surface. Moreover, it can be observed that the carbonization of the CB and CP samples resulted in the increase of quaternary nitrogen (BE = 401.4 eV), due to the condensation reactions during the carbonization (Raymundo-Piñero *et al.*, 2002).

Table 4.3 Deconvolution results of XPS C1s, O1s and N1s peaks for AC before and after surface treatment

Region	Position (eV)	Intensity (%)					Assignment
		AC	ACO10-6	ACO10-8	ACO10-12	ACN400	
C1s	284.3±0.1	47.9	43.2	44.0	39.4	44.9	Graphite
	285.0±0.1	25.2	15.9	18.3	23.0	24.8	Aliphatics
	285.4±0.2	0.0	9.2	9.7	10.2	10.1	Carbons linked to nitrogen
	285.8±0.1	6.5	10.3	9.1	9.6	7.1	Hydroxyl, Ether
	286.6±0.2	7.6	10.0	11.4	12.7	9.7	Carbonyl
	289.2	12.7	11.4	7.6	5.0	3.5	Esters, Lactones, Anhydrides, Acids, Hydroxyl
O1s	530.3	3.9	2.0	3.0	7.4	4.7	Oxides
	531.3±0.1	13.3	24.8	26.3	27.8	9.3	Carbonyl, Carboxyl
	532.1±0.1	27.0	28.8	21.8	18.9	25.4	Ketones, Lactones, Acids, Esters
	532.9±0.1	20.0	30.6	31.4	17.5	21.5	Hydroxyl, Carboxyl
	533.6±0.1	28.8	13.8	12.4	21.9	31.2	Hydroxyl attached to aromatic ring, oxygen in bridge (esters)
	534.9±0.1	6.2	0.0	5.2	6.6	7.9	Adsorbed water
N1s	398.1±0.1	0.0	7.6	3.2	6.2	3.5	Pyridinic
	398.9±0.1	0.0	27.6	32.4	36.4	16.4	Pyridinic, Imine
	399.8±0.2	0.0	25.8	45.6	38.6	21.7	Imine, Amide, Amine
	400.7±0.2	0.0	18.5	13.4	6.2	28.5	Pyrrolic, Pyridonic
	401.4±0.3	0.0	9.8	5.3	12.7	23.2	Quaternary nitrogen
	402.8±0.2	0.0	10.7	0.0	0.0	6.6	Pyridine-N-oxide

Table 4.3 Deconvolution results of XPS C1s, O1s and N1s peaks for AC before and after surface treatment (cont'd)

Region	Position (eV)	Intensity (%)					Assignment
		ACN 600	ACN 800	ACO10-6 /N400	ACO10-8 /N400	ACO10-12 /N400	
C1s	284.3±0.1	45.7	46.5	40.7	44.2	43.9	Graphite
	285.0±0.1	23.1	22.8	17.9	18.2	19.4	Aliphatics
	285.4±0.2	9.3	6.9	10.9	10.8	11.2	Carbons linked to nitrogen
	285.8±0.1	9.5	7.9	7.5	11.4	10.1	Hydroxyl, Ether
	286.6±0.2	9.5	9.3	13.7	9.2	10.0	Carbonyl
	289.2	2.9	6.5	9.3	6.2	5.5	Esters, Lactones, Anhydrides, Acids, Hydroxyl
O1s	530.3	6.6	3.9	6.3	5.6	4.4	Oxides
	531.3±0.1	10.3	16.0	17.2	19.5	20.7	Carbonyl, Carboxyl
	532.1±0.1	19.8	23.1	40.2	30.4	20.9	Ketones, Lactones, Acids, Esters
	532.9±0.1	18.7	26.6	23.6	20.2	23.0	Hydroxyl, Carboxyl
	533.6±0.1	38.2	26.6	12.7	20.1	25.7	Hydroxyl attached to aromatic ring, Oxygen in bridge (esters)
	534.9±0.1	6.4	4.3	0.0	4.4	5.4	Adsorbed water
N1s	398.1±0.1	6.9	0.0	4.6	6.0	2.8	Pyridinic
	398.9±0.1	19.2	26.5	15.1	19.5	15.9	Pyridinic, Imine
	399.8±0.2	6.5	33.1	26.8	25.5	32.8	Imine, Amide, Amine
	400.7±0.2	25.3	11.1	22.9	27.6	32.2	Pyrrolic, Pyridonic
	401.4±0.3	22.6	19.9	20.2	14.5	10.8	Quaternary nitrogen
	402.8±0.2	19.5	9.4	10.5	6.8	5.6	Pyridine-N-oxide

Table 4.4 Deconvolution results of XPS C1s, O1s and N1s peaks for ACB before and after surface treatment

Region	Position (eV)	Intensity (%)					Assignment
		CB	ACB	ACBO 10-12	ACBN400	ACBO 10-12/N400	
C1s	284.3±0.1	67.7	53.8	45.3	42.2	49	Graphite
	285.0±0.1	22.3	20.3	15.9	22.6	12.9	Aliphatics
	285.4±0.2	0.0	0.0	5.6	6.9	8.0	Carbons linked to nitrogen
	285.8±0.1	0.0	6.6	7.5	8.4	5.7	Hydroxyl, Ether
	286.6±0.2	9.0	9.5	9.1	9.1	9.4	Carbonyl
	289.2	0.0	9.9	16.5	10.8	15	Esters, Lactones, Anhydrides, Acids, Hydroxyl
O1s	530.3	0.0	6.0	9.5	9.2	6.1	Oxides
	531.3±0.1	0.0	18.6	25.5	13.2	23.1	Carbonyl, Carboxyl
	532.1±0.1	0.0	27.1	24.4	31.8	24.3	Ketones, Lactones, Acids, Esters
	532.9±0.1	0.0	21.8	8.9	11.7	9.9	Hydroxyl, Carboxyl
	533.6±0.1	0.0	26.5	26.2	28.4	31.1	Hydroxyl attached to aromatic ring, oxygen in bridge (esters)
	534.9±0.1	0.0	0.0	5.5	5.7	5.1	Adsorbed water
N1s	398.1±0.1	0.0	0.0	2.3	11.1	10.4	Pyridinic
	398.9±0.1	0.0	0.0	9.5	13.9	16.4	Pyridinic, Imine
	399.8±0.2	0.0	0.0	40.2	18.3	18.9	Imine, Amide, Amine
	400.7±0.2	0.0	0.0	28.9	26.6	31.7	Pyrrolic, Pyridonic
	401.4±0.3	0.0	0.0	19.1	23.1	20.1	Quaternary nitrogen
	402.8±0.2	0.0	0.0	0.0	7.1	2.5	Pyridine-N-oxide

Table 4.5 Deconvolution results of XPS C1s, O1s and N1s peaks for ACP before and after surface treatment

Region	Position (eV)	Intensity (%)					Assignment
		CP	ACP	ACPO 10-12	ACPN400	ACPO 10-12/N400	
C1s	284.3±0.1	50.8	50.3	40.0	40.1	42.4	Graphite
	285.0±0.1	15.9	14.2	19.0	17.2	17.0	Aliphatics
	285.4±0.2	15.3	6.3	8.6	8.9	11.1	Carbons linked to nitrogen
	285.8±0.1	11.0	6.5	10.2	8.5	7.9	Hydroxyl, Ether
	286.6±0.2	6.9	13.2	10.7	9.4	11.2	Carbonyl
	289.2	0.0	9.5	11.6	16.0	10.4	Esters, Lactones, Anhydrides, Acids, Hydroxyl
O1s	530.3	0.0	3.9	4.9	6.3	5.2	Oxides
	531.3±0.1	0.0	18.5	29.0	10.8	31.1	Carbonyl, Carboxyl
	532.1±0.1	0.0	38.1	12.9	37.4	30.2	Ketones, Lactones, Acids, Esters
	532.9±0.1	0.0	16.6	23.1	13.7	16.1	Hydroxyl, Carboxyl
	533.6±0.1	0.0	19.4	20.4	25.8	14.2	Hydroxyl attached to aromatic ring, oxygen in bridge (esters)
	534.9±0.1	0.0	3.6	9.6	6.1	3.1	Adsorbed water
N1s	398.1±0.1	14.3	6.3	9.5	14.1	16.8	Pyridinic
	398.9±0.1	47.9	38.4	34.3	12.7	13.5	Pyridinic, Imine
	399.8±0.2	19.7	13.8	31.4	25.0	12.5	Imine, Amide, Amine
	400.7±0.2	12.4	19.3	12.8	30.0	34.8	Pyrrolic, Pyridonic
	401.4±0.3	5.7	18.7	7.0	13.0	17.2	Quaternary nitrogen
	402.8±0.2	0.0	3.5	5.0	5.3	5.1	Pyridine-N-oxide

4.2 CO_2 Adsorption Performance

The CO_2 adsorption capacity at 40 °C and 1 atm, obtained by a gravimetric technique undertaken in the simultaneous thermal analyzer, is listed in Table 4.6.

Table 4.6 The CO_2 adsorption capacities at 40 °C and 1atm of the studied samples

Sample	CO_2 Adsorption Capacity wt% (mmol/g sorbent)
AC	5.93 (1.35)
ACO10-6	6.31 (1.43)
ACO10-8	7.03 (1.60)
ACO10-12	7.68 (1.75)
ACN400	6.48 (1.47)
ACN600	6.21 (1.41)
ACN800	5.23 (1.19)
ACO10-6/N400	6.78 (1.54)
ACO10-8/N400	7.56 (1.72)
ACO10-12/N400	7.73 (1.76)
CB	1.50 (0.34)
ACB	3.99 (0.91)
ACBO10-12	4.95 (1.13)
ACBN400	4.55 (1.03)
ACBO10-12/N400	6.12 (1.39)
CP	0.00 (0.00)
ACP	5.02 (1.14)
ACPO10-12	5.52 (1.25)
ACPN400	5.41 (1.23)
ACPO10-12/N400	5.63 (1.28)

4.2.1 Effect of Oxidative Duration on CO_2 Capture Performance

CO_2 adsorption/desorption profile was plotted with mass uptake percentages versus times. Figure 4.3 exhibits a comparison of the CO_2 adsorption/desorption profiles of the untreated AC and AC after treatment by 10 M HNO_3 at different oxidation duration (6, 8, and 12 hours). The untreated AC has a CO_2 capture capacity of 1.35 mmol/g. It is clearly seen from the figure that the oxidized AC can adsorb more CO_2 than the untreated AC. The ACO10-12 exhibited the largest enhancement in CO_2 capacity (1.75 mmol/g) followed by ACO10-8 (1.60 mmol/g) and ACO10-6 (1.43 mmol/g), respectively.

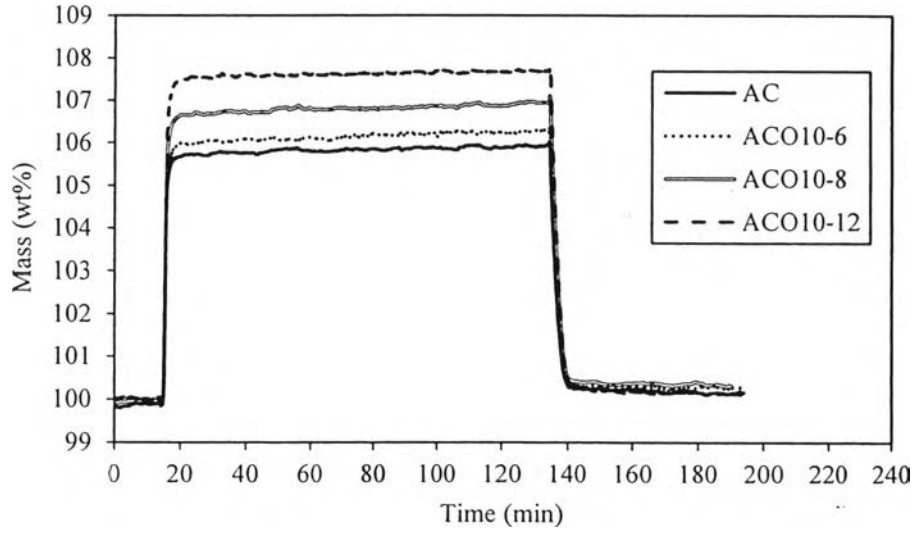

Figure 4.3 CO_2 adsorption/desorption profiles (40 °C) of AC treated by HNO_3 oxidation at various durations.

It is obvious that the higher amount of oxygen functional groups introduced into the carbon sample led to the better CO_2 adsorption. The presence of oxygen surface groups was investigated by XPS analysis, which showed that the HNO_3 oxidation introduced mainly carbonyl or carboxyl groups into the carbon surface. Beside the nitrogen containing groups, the oxygen containing groups can also present the ability to interact with CO_2 molecules, especially carboxyl group (Xing *et al.*, 2014). The carboxyl groups contain not only carbonyls (C=O) that can behave as a Lewis base to the carbon atom (Lewis acid) in CO_2 molecule, but also acidic proton (H^+) that can behave as Lewis acid to the oxygen atoms (Lewis bases) in the CO_2

molecule (Plaza *et al.*, 2013). Therefore, the samples with higher amount of these groups gave the greater interaction between CO_2 molecules and carbon surface.

4.2.2 Effect of Amination Temperature on CO_2 Capture Performance

The adsorption/desorption profiles of the untreated AC and AC after treated by ammonia at various temperature (400, 600, and 800 °C) are compared in Figure 4.4. The amount of CO_2 capture by AC treated under ammonia atmosphere at 400 °C and 600 °C (1.47 mmol/g for ACN400 and 1.41 mmol/g for AN600) were greater than the untreated AC (1.35 mmol/g). Whereas, the sample with ammonia treatment at 800 °C resulted in the decrease of CO_2 adsorption capacity.

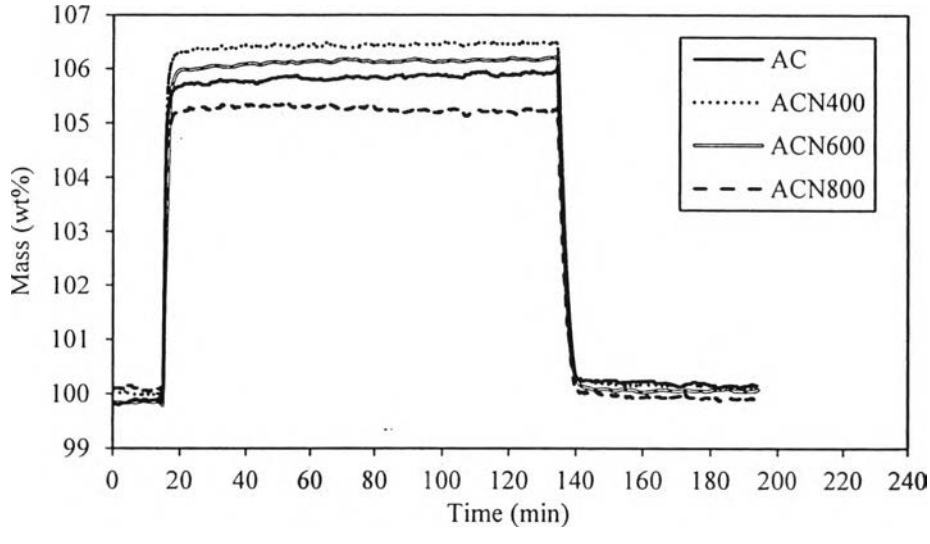

Figure 4.4 CO_2 adsorption/desorption profiles (40 °C) of AC treated by amination at various temperature.

The CO_2 capture capacity enhancement of the ACN400 and ACN600 samples could be ascribed to the basic nature on the surface of aminated samples. The basic nitrogen functionalities can be introduced into the carbon structure by amination as confirmed by XPS study. The XPS analysis indicated the presence of pyridinic, imine, amide, amine, pyrrolic, pyridonic, quaternary nitrogen, and pyridine-N-oxide of the aminated samples. The pyrrolic and pyridonic groups, which corresponded to the strong basic nature, were mainly incorporated. These basic site as

Lewis base can react with CO_2 as Lewis acid leading to an increase in CO_2 adsorption (Przepiórski *et al.*, 2004; Pevida *et al.*, 2008a; Shafeeyan *et al.*, 2011). Among the samples treated by amination, ACN800 contained the smallest nitrogen introduced. According to the XPS results, the major species found on the 800 °C aminated sample were imine, amide or amine groups. These surface functional groups might cause the weak interaction between CO_2 gas and carbon surface compared to the strong basic sites such as the pyrrolic and pyridonic groups.

4.2.3 Effect of Pre-oxidation on CO_2 Capture Performance

The CO_2 adsorption profiles of AC treated by various approaches (see Figure 4.5) show that the samples treated with oxidation followed by amination method showed the higher amount of CO_2 adsorption compared to the sample treated by amination without pre-oxidation. This suggested that the oxidation of AC before amination can improve the ability to adsorb CO_2 of AC treated by amination alone. The CO_2 capacity increased from 1.47 mmol/g of ACN400 to 1.54, 1.72, and 1.76 mmol/g of ACO10-6/N400, ACO10-8/N400, and ACO10-12/N400, respectively.

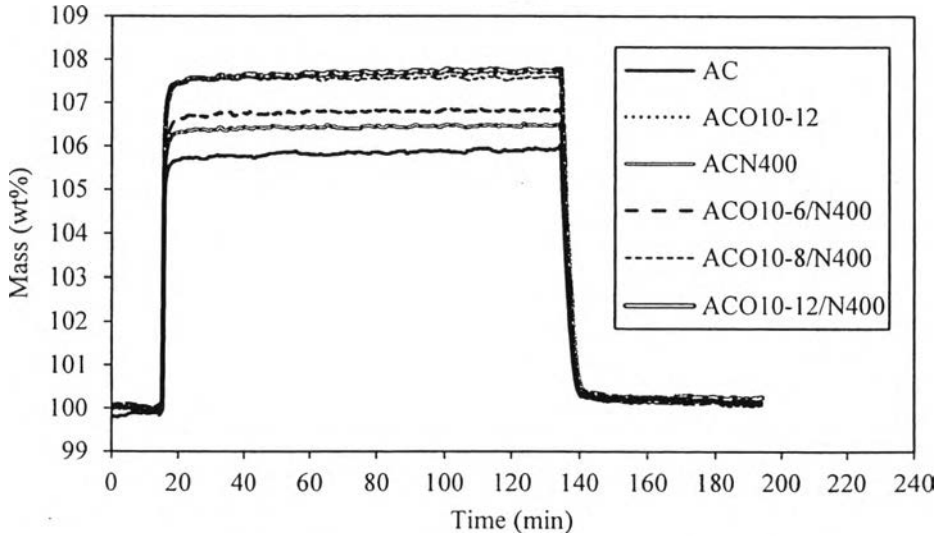

Figure 4.5 CO_2 adsorption/desorption isotherms (40 °C) of AC treated by oxidation, amination without pre-oxidation, and amination with pre-oxidation.

The largest CO_2 uptake belonged to the AC treated by 400 °C amination with the highest oxygen groups formed by HNO_3 pre-oxidation (ACO10-12/N400). This indicates that the higher amount of oxygen functionalities prior to amination could help create more nitrogen groups on the carbon surface, promoting the interactions between basic nitrogen groups and acidic CO_2.

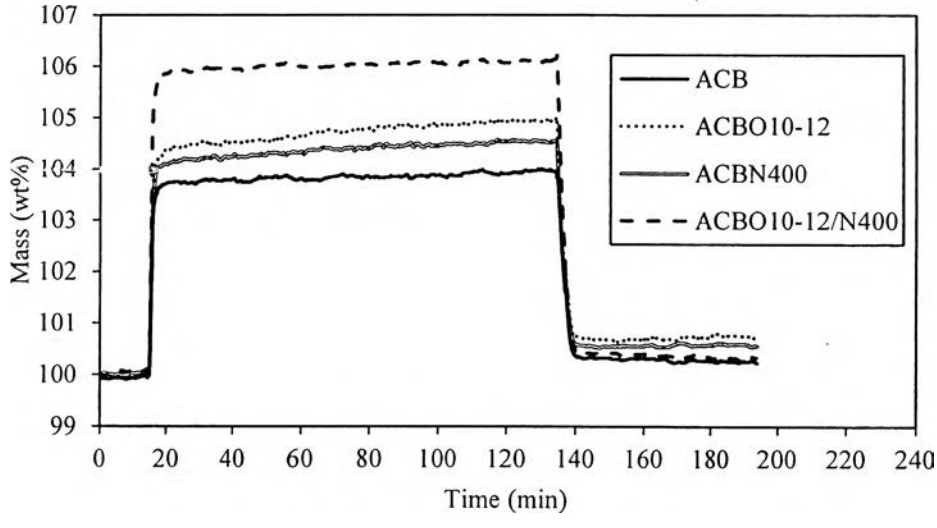

Figure 4.6 CO_2 adsorption/desorption isotherms (40 °C) of ACB treated by oxidation, amination without pre-oxidation, and amination with pre-oxidation.

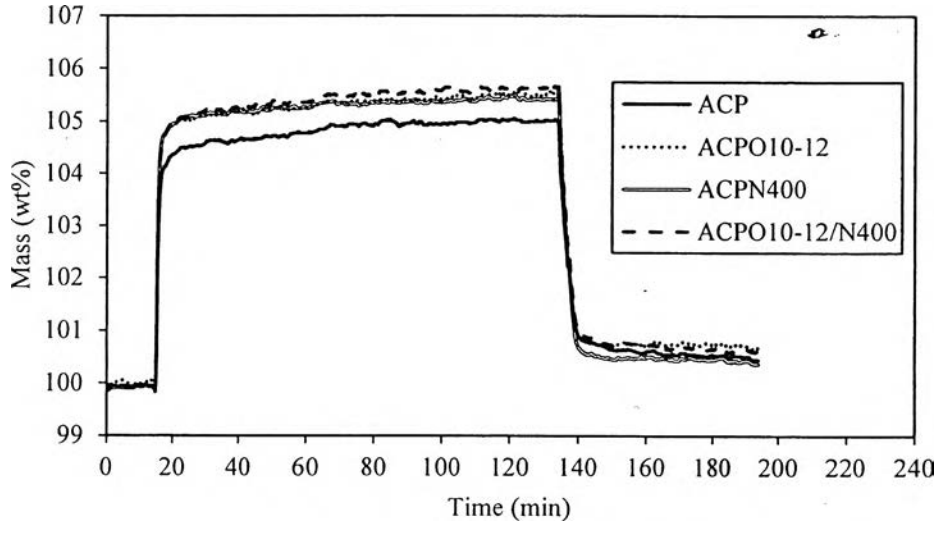

Figure 4.7 CO_2 adsorption/desorption isotherms (40 °C) of ACP treated by oxidation, amination without pre-oxidation, and amination with pre-oxidation.

A similar trend was observed for ACB and ACP treated by various approaches (Figures 4.6 and 4.7) that the highest amount of CO_2 uptake belonged to both carbons treated by amination with pre-oxidation method (1.39 mmol/g for ACBO10-12/N400 and 1.28 mmol/g for ACPO10-12/N400). Therefore, it can be conclude that the active oxygen functionalities from HNO_3 pre-oxidation created more sites for free radicals from NH_3 treatment to form nitrogen functionalities on the carbon surface, favoring the Lewis acid–Lewis base interactions between CO_2 molecules and nitrogen (Shafeeyan *et al.*, 2011; Adelodun *et al.*, 2013).

4.2.4 Effect of Different Activated Carbon on CO_2 Capture Performance

Table 4.6 shows that the starting carbon (CB and CP) are not suitable materials for CO_2 adsorption. This is due to their low micropores which is responsible for physical adsorption (Plaza, 2009c). The CB sample gave a very low adsorption capacity of 0.34 mmol/g, while there was no CO_2 adsorbed on the CP sample. It was evidenced in Table 4.1 that micropores were created after carbonization and activation (i.e. CB versus ACB and CP versus ACP). Therefore, the amount of CO_2 uptake of CB and CP increased to 0.91 mmol/g and 1.14 mmol/g, respectively. The CO_2 adsorption/desorption profiles of AC, ACB, and ACP samples are compared in Figure 4.8. In comparison, the AC sample showed the greatest amount of adsorbed CO_2 (1.35 mmol/g) followed by ACB (1.14 mmol/g) and ACP (0.91 mmol/g), respectively. This is due to the AC sample presented the largest micropores. However, it can be observed that the ACB sample gave a lower CO_2 capacity than that of ACP although ACB possessed greater micropore volume. This indicated that the surface chemistry played a dominant role in determining the CO_2 uptake of ACP. The XPS analysis showed that the ACP sample presented various types of nitrogen surface functionalities including pyridinic, imine, amide, amine, pyrrolic, pyridonic, quaternary nitrogen, and pyridine-N-oxide, which are responsible for basic nature that allows the increase of affinity of carbon toward acidic CO_2 (Przepiórski *et al.*, 2004; Pevida *et al.*, 2008a; Shafeeyan *et al.*, 2011). Whereas there was no nitrogen groups present on ACB sample, therefore it exhibited only physical adsorption of CO_2 on the surface.

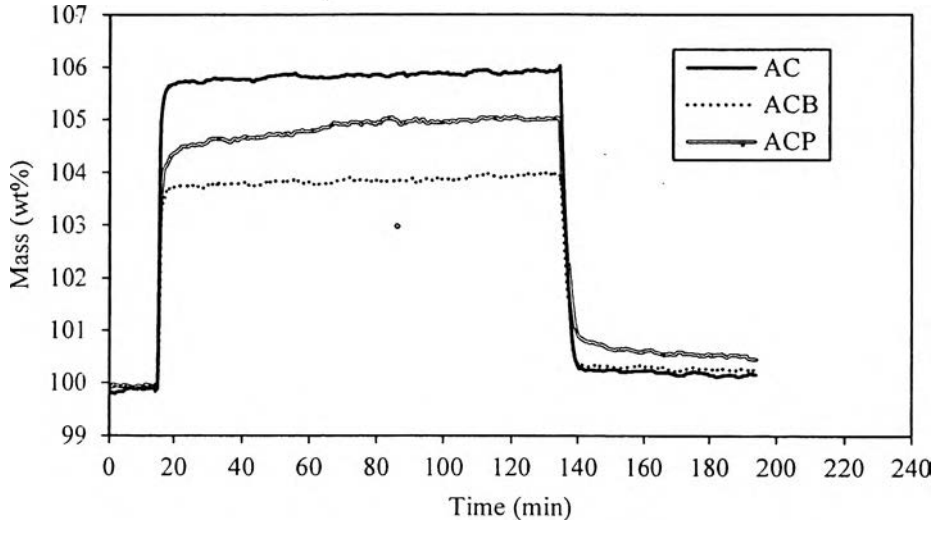

Figure 4.8 CO_2 adsorption/desorption profiles (40 °C) of AC, ACB, and ACP.